# REPORT DOCUMENTATION PAGE

*Form Approved OMB No. 0704-0188*



| 1. REPORT DATE *(30-12-2007)* | 2. REPORT TYPE final | 3. DATES COVERED *(From -To)* 01/01/2007-09/30/2007 |
|---|---|---|

**4. TITLE AND SUBTITLE** STRUCTURAL WAVEGUIDES FOR AERODYNAMIC TURBULENT DRAG REDUCTION

**5a. CONTRACT NUMBER FA9550-07-10064**

**5b. GRANT NUMBER N/A**

**5c. PROGRAM ELEMENT NUMBER N/A**

**6. AUTHOR(S)** Pavlos P. Vlachos, Martin Johnson, Alessandro Toso, James Carneal

**5d. PROJECT NUMBER N/A**

**5e. TASK NUMBER N/A**

**5f. WORK UNIT NUMBER n/A**

**7. PERFORMING ORGANIZATION NAME(S) AND ADDRESS(ES)**
**Mechanical Engineering Dept.100 Randolph Hall Blacksburg,VA, 24061Virginia Tech**

**8. PERFORMING ORGANIZATION REPORT NUMBER** One (1)

**9. SPONSORING / MONITORING AGENCY NAME(S) AND ADDRESS(ES)**
**AFOSR**
875N Randolph St, Ste 325
Arlington VA 22203
Director Gaurguctu/NA

**10. SPONSOR/MONITOR'S ACRONYM(S) N/A**

**11. SPONSOR/MONITOR'S REPORT NUMBER(S)** N/A

**12. DISTRIBUTION / AVAILABILITY STATEMENT**Available for public distribution

Approved for public release,
distribution unlimited

AFRL-SR-AR-TR-08-0048

20080131276

**13. SUPPLEMENTARY NOTES N/A**

**14. ABSTRACT** The objective of this project was to provide a proof-of-concept that travelling wavedisturbances on the surface of a vehicle can generate viscous drag reduction benefits. Thiswould be accomplished by developing structural waveguides within a cylinder that underactuation impart a structural surface wave disturbance in the form of a travelling wave.During the nine month performance of the work presented herein we were successful indesigning and fabricating structural waveguides. Structural characterization of the prototypedemonstrates that the performance met the design expectation. Subsequently, initial aerodynamic testing was performed in order to validate that the proposed concept can impartflow disturbances that reduce turbulent viscous drag. At the time of this report onlyquantitative flow visualization under quiescent flow conditions had been performed and preliminary analysis of the results is presented. The PIV results showed a three stage cycleoccurring, which creates a motion that sweeps the flow very close to the wall in a clockwisedirection. This movement of fluid might interrupt the near-wall turbulence production and

**15. SUBJECT TERMS Structural waveguides, active flow control, drag reduction**

| 16. SECURITY CLASSIFICATION OF: | | 17. LIMITATION OF ABSTRACT | 18. NUMBER OF PAGES | 19a. NAME OF RESPONSIBLE PERSON Pavlos P. Vlachos | | |
|---|---|---|---|---|---|---|
| a. REPORT | | | 25 | b. ABSTRACT | c. THIS PAGE | 19b. TELEPHONE NUMBER *(include area code)*540 231-3366 |

# STRUCTURAL WAVEGUIDES FOR AERODYNAMIC TURBULENT DRAG REDUCTION

BY

BY PAVLOS VLACHOS, MARTY JOHNSON, JAMES P CARNEAL, AND ALESSANDRO TOSSO

VIRGINIA TECH MECHANICAL ENGINEERING DEPARTMENT

BLACKSBURG, VA 24060

TO: TECHNICALREPORTS@AFOSR.AF.MIL

SUBJECT: FINAL PROGRESS STATEMENT TO DR GIURGIUTIU, VICTOR

CONTRACT/GRANT #: FA9550-07-10064

REPORTING PERIOD: JAN 1 2007 SEPT 30 2007

ACCOMPLISHMENTS (200 WORDS):

The objective of this project was to provide a proof-of-concept that travelling wave disturbances on the surface of a vehicle can generate viscous drag reduction benefits. This would be accomplished by developing structural waveguides within a cylinder that under actuation impart a structural surface wave disturbance in the form of a travelling wave. During the nine month performance of the work presented herein we were successful in designing and fabricating structural waveguides. Structural characterization of the prototype demonstrates that the performance met the design expectation. Subsequently, initial aerodynamic testing was performed in order to validate that the proposed concept can impart flow disturbances that reduce turbulent viscous drag. At the time of this report only quantitative flow visualization under quiescent flow conditions had been performed and preliminary analysis of the results is presented. The PIV results showed a three stage cycle occurring, which creates a motion that sweeps the flow very close to the wall in a clockwise direction. This movement of fluid might interrupt the near-wall turbulence production and reduce the viscous drag. Future work on this project will include wind tunnel drag measurements in order to investigate the effect of the travelling wave on the turbulent viscous drag.

ARCHIVAL PUBLICATIONS (PUBLISHED) DURING REPORTING PERIOD: NONE

CHANGES IN RESEARCH OBJECTIVES: NONE

CHANGE IN AFOSR PROGRAM MANAGER: NONE

EXTENSIONS GRANTED OR MILESTONES SLIPPED: NONE

## CONTENTS

## INTRODUCTION

Recent analytical investigations suggest that a reduction in wall bounded turbulent drag can be achieved by the action of a transverse traveling wave via surface deflections. The reduction in drag can be up to 40% which could eventually lead to significant improvements in aircraft efficiency. This work has mostly been verified analytically since the actuator parameters (forces, displacement, and frequency range) required for this traveling wave are beyond standard actuator capabilities.

This effort pursued the investigation and development of structural waveguides that have potential to meet these specifications and experimentally explored the ability for drag reduction. A structural waveguide can be theoretically produced in any structure by controlling the boundary conditions to make the structure look "continuous". This can be accomplished by a combination of intelligent structural design coupled with piezoelectric, piezopolymer, electro-expulsive, or other embedded smart material actuators. Circular structures are well-suited for propagating waves since they are inherently continuous. This leads directly to application on aircraft fuselages, where the propagating wave in the circular structure will be inherently parallel to the flow. Smart material actuators using phased array drive concepts can be applied to the structure to excite the traveling waves. The structural waveguide concepts were analytically and experimentally investigated. This was a one year proof-of concept preliminary study.

The design and fabrication of the structural waveguides was completed successfully and structural characterization of performance confirmed the expected results. A summary of these results will be provided in the flowing sections. At the end of the project, preliminary aerodynamic validation of the concepts was pursued on a cylindrical structure instrumented with a full array of flow visualization, vibration and drag measurement equipment. Upon completion of the performance period of the project and during the authorship of the present report, the aerodynamic experiments were still in process. Further experiments analysis and detailed dissemination of the aerodynamic testing results will be presented in future/upcomming conference proceedings and archival journal publications.

This was a multidisciplinary effort between faculty of the Mechanical engineering Department at Virginia Tech. Drs James Carneal and Marty Johnson of the Vibrations and Acoustics Lab provided expertise in structural dynamics, phased array actuators/sensors, and novel actuators for active noise and vibration control, and Dr Pavlos Vlachos provided the expertise in fluid dynamics and experimental flow diagnostics.

The research presented herein is original and risky. The preliminary results indicate that the proposed concept is feasible and offer scientific and practical engineering merit. Continuation of this effort has the potential for significant scientific, social and economic impact and commercial applications. Almost all wall bounded flows and fluid machinery are subject to wall turbulence. Efficient control of the character of the flow will save energy, improve performance, and open new prospects for engineering applications.

## BACKGROUND:

In the following section, background work is summarized and presented in two main areas: turbulence control theory and structural waveguides. However, extensive review of this topics is beyond the scope of this document as well as review of topics related to smart material actuators, and phased array actuators.

### TURBULENCE CONTROL THEORY

Numerous flow control methodologies have been employed to favorably alter flow behavior. Applications include flow control of separation, separated flows, circulation, as well as lift increase and drag reduction. All these technologies, upon maturation, can potentially have significant impact to a variety of vehicle platforms and fluid machinery. Among these, turbulent boundary layer control towards viscous drag reduction has been a formidable area of research. A thorough review of this topic is beyond the scope and the page limitations of this text. We will however review and discuss some of the most recent and significant contributions as they pertain to the effort proposed herein.

The development of modern turbulence control mechanisms and the corresponding shear stress reduction depends upon the observation that organized structures in the near-wall region and the friction drag are inevitably linked [1]. Two key elements of this view have been the discovery of low speed streaks in turbulent boundary layers as well as the verification of Theodorsen's hypothesis on the existence of stable three-dimensional vortical structures, called hairpins [2]. More specifically, vortex pairs (loops) and horseshoe or hairpin-like vortices have been recognized as the dominant flow structures in the near-wall region of turbulent boundary layers, and many researchers have colorfully described boundary layers as a "forest" or a "jungle" of hairpins [3].

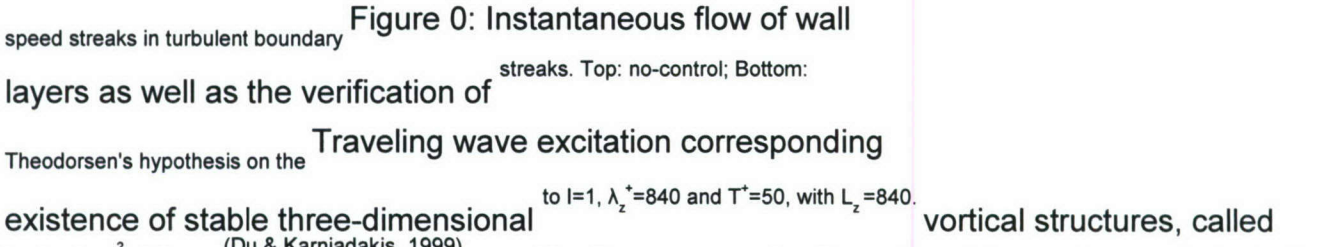

Figure 0: Instantaneous flow of wall streaks. Top: no-control; Bottom: Traveling wave excitation corresponding to l=1, $\lambda_z^+$=840 and $T^+$=50, with $L_z$=840. (Du & Karniadakis, 1999)

In this effort we are interested in the mechanisms of modifying the above-described structure of the turbulent boundary layer. Karniadakis & Choi [4] provide the most up-to-date and extensive review on flow control of turbulent boundary layers via transverse actuations. Methods for near-wall turbulence control have been developed under the assumption that the turbulence production cycle could be favorably altered by the manipulation, stabilization or suppression of low-speed streaks, quasi-streamwise vortices or the hairpin-like structures that populate the near-wall region. Small grooves or riblets mounted on the wall surface have proved to be effective in partially suppressing turbulence and reducing the drag force by about 5% to 10% [5-8]. Additional promise was demonstrated by flow control using wall oscillations as an alternative effective mechanism for drag reduction [9-12]. Drag reduction as much as 40% was demonstrated experimentally by Choi et al [10].

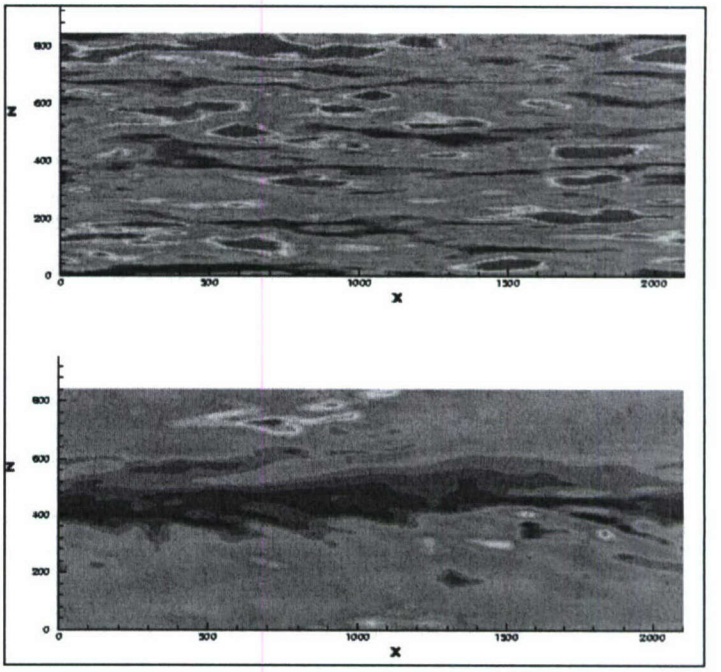


Despite successful demonstration of drag reduction methodologies, the fundamental understanding of the governing dynamics remains a great challenge. Significant contributions by Jimenez & Pinelli[13] and Schoppa & Hussain[14] have shed light on the self-sustained processes of wall-turbulence and demonstrated numerically that the turbulence regeneration cycle is exclusively associated with the near-wall region and is independent of the outer flow. Schoppa & Hussain later used this concept to propose a large-scale drag reduction technique employing vortex generators along the channel centerline, which resulted in drag reduction on the order of 20-60%[15]. Subsequently, they were able to identify a new mechanism for the transient growth of streak instabilities[16]. These contributions, among others, provide an established relationship between streamwise vorticity, streak instability and vortex-induced viscous drag. Subsequent work revealed a fundamental mechanism which completely eliminates these near-wall streaks[17,18]. Using numerical simulations Du & Karniadakis proposed a flow control method based on the application of a body force acting within the viscous sublayer and decaying exponentially away from the wall, traversing the flow in the spanwise direction in the form of a traveling wave. In particular, the following traveling wave force, *Fz, is introduced:*

$$F = Ie^{-\frac{y}{\delta}} \sin\left(\frac{2\pi z}{\lambda} - \frac{2\pi t}{T}\right) \quad \text{Equation 1}$$

where I is the amplitude of excitation, λ is the wavelength (along the span), and T is the time period. Here $\Delta^{+}=U_{*}\Delta/\nu$, where $U_{*}$ is the wall shear velocity and ν is the kinematic viscosity ("+" as a superscript indicates that the quantity is expressed in viscous wall units).

For channel flow, it is shown in Figure 0 (z : spanwise direction) that the uncontrolled case

exhibits the familiar turbulence structure consisting of pairs of high-speed and low-speed streaks, but no such pairs can be found near the controlled surface. The resulting overall drag reduction from this simulation was in excess of 30%. This is a significant finding, in view of the fact that streaks and streak spacing are usually difficult to alter, even in cases where a very large amount of drag reduction has been obtained as in drag reduction using polymer or bubble injections. **All previous methods were unable to eliminate the near wall streaks, whereas this technique accomplishes exactly that.**

Addressing the energetics associated with this turbulence control methodology, it has been found via systematic DNS experimentation [18] that the specific waveform, i.e. the parameters T, λ, I, are critical in obtaining turbulence suppression and corresponding drag reduction. They hypothesized that it is the total amount of energy input that is critical in suppressing turbulence, and this can be expressed by the product $\mathbf{I \times T^+}$. This quantity represents an energy invariant parameter and it has been demonstrated that there is an optimum regime of energy input, outside which the control has either no effect or results in promoting turbulence. For practical applications this is very important as it suggests that the flow control is not only robust but is also forgiving in the sense that there is not a unique input condition that will have positive ramifications. Any product of I and $T^+$ that satisfies the energy requirement should be effective. **The implications of this are that this aerodynamic flow control method is open-loop, i.e. the control system does not need estimates of the plant, nor does it need upstream sensors to correctly phase the structural waveguide with the flow perturbations.** It appears that this optimum regime is a function of the Reynolds number and as a result for optimum control the penetration length needs to be determined from the reciprocal of the *energy invariant product*:

$$\Delta \approx \text{Const} \times (I \times T+)\text{-}1. \quad \text{Equation 2}$$

From Du[17], these non-dimensional parameters can be applied to aerodynamic turbulent drag reduction, resulting in wavelengths on the order of 20-200 mm, and pulsing frequencies on the order of 50-500 Hz.

The hypothesis of this invariant product has been tested extensively numerically, however to date no experimental proof has been established. There is very little information available for experiments employing an electromagnetic traveling wave force. Karniadakis and Choi[4] state that there were no journal papers available at that time; however they report on a few ongoing preliminary efforts. Recently Park et al[19] and Breuer et al[20] reported on Lorentz force actuator development and drag reduction experiments using direct force balance measurements. This preliminary study was limited to very low free-stream velocities, and a drag reduction on the order of 9% was found. However, the mechanical efficiency was approximately $10^{-4}$ which is unacceptable for any practical applications. Their detailed study illustrated several problems related to the implementation of a Lorenz force actuation scheme such as corrosion, bubble formation, and low induced velocities. Reportedly, the efficiency increases for high Reynolds numbers (Prof. Karniadakis, personal communication); however, these efforts are still in progress and many questions remain unanswered.

Inspired by these previous efforts, this work explores an alternative methodology for turbulent boundary layer flow control that overcomes the limitations of the Lorenz force actuation. **A flow disturbance in the form of a traveling wave force generated by a structural waveguide is used to manage the near wall turbulent flow.** This innovative concept overcomes some of the shortcomings of the electromagnetic force such as corrosion or bubble formation, and more

importantly is independent of the conductivity of the fluids, thus applicable to both air and water flows. Although implementation concepts have been proposed before[21], no published results, experimental or numerical, of turbulent boundary layer flow control using these concepts currently exist. Moreover, the mechanism of the proposed flow control is based on modifying or interrupting the self-sustaining cycle of near-wall turbulence. Therefore, in contrast to previous successful flow control approaches, the present methodology tackles the fundamental mechanisms of near wall turbulence.

## STRUCTURAL WAVEGUIDE CONCEPTS

Analysis of a structural waveguide is a fundamental analysis of distributed elastic system flexural vibration, where the beam/plate is assumed infinite and a wave is free to propagate in all directions. The inclusion of finite boundary condition to this model will result in modal behavior, which is a result of the wave bouncing off the boundaries, which occurs when the propagating wave encounters a change in impedance. Physically, structural waveguides exist in circular structures since they are continuous and have no boundary[22,23]. From Fahy[23], the axial, tangential, and radial displacements (u,v,w) of the wall of a cylinder vary with the axial position $z$ and the azimuth angle θ, can be written as:

$$u,\ v,\ \mathrm{w} = [\mathrm{U}\ (z), \mathrm{V}\ (z), \mathrm{W}\ (z)]\cos(n\theta + \theta) \quad \text{Equation 3}$$

for $n \geq 0$. From the above equation, it is obvious that the **cylinder supports standing waves in the circumferential direction, with** n **integer waves**.

Excitation of the structural waveguide can be accomplished via embedded smart material actuators. The field of embedded smart material actuators is quite extensive[24,25,26]. Piezoelectric actuators can be bonded to a structure and can produce an in-plane strain on the structure when driven electrically. There is a plethora of research on these actuators bonded to structures and they have been applied to such diverse fields as active noise control and control of helicopter blade aerodynamics. Excitation of a cylinder by a piezoelectric actuator is derived in Lalande[27,28]. The piezoelectric actuator is viewed as a distributed in-plane strain forcing function. To arrive at a particular solution for a cylinder with rigid boundary conditions, this forcing function is decomposed into the modal eigenfunctions of the cylinder, generating modal participation factors for the actuator. To accomplish a propagating traveling wave in a cylindrical structure excited by embedded smart material actuators, phased array actuators were employed[29,30]. The main concept is that multiple sensors/actuators can be used in unison to create an array that is particularly sensitive in one spatial domain, in this instance, the modal domain. To excite specific structural modes, several actuators can be driven in a spatial phased array[31]. These actuators will be driven with a spatial phase array concept where the signal driving one actuator will be delayed by a time (Δt) that will reinforce the wave propagating from the previous actuator[32]. By repeating this concept N times, the phased array actuator generates only one traveling wave corresponding to the actuator spacing and time delay.

Non-circular structures are finite and will therefore exhibit modal behavior. Recently, there have been efforts to model waveguides with arbitrary cross-sections, periodic structures, and in-homogeneities[33,34,35]. Therefore, one significant challenge is to design non-circular structures which posses these properties e.g. similar shape to an airfoil. One potential solution is to apply embedded smart materials that can create and absorb waves in the finite structure that will match the impedance of the "infinite" structure at the boundaries. This can also be

accomplished passively using a distributed vibration absorber[36], which can effectively absorb specific wavenumbers in the structure. However, an investigation into non-cylindrical waveguides was not pursued because of the time and financial constraints of this project.

## STRUCTURAL WAVEGUIDE AND TEST RIG DESIGN

The test rig has been designed in order to represent as close as possible a simply supported cylinder. For this configuration, an analytical solution is available for the normal modes.

In the literature it is possible to find different formulations for the description of the cylinder dynamics that are valid for several boundary condition and cylinder properties. In this study we have focused on thin walled structures where the ratio between the thickness of the cylinder and its diameter is small.

If we consider an infinite cylinder, the equation of motion for axial, radial and torsional direction, are highly coupled unlike the case of plates and beams. The solution in terms of displacement in the three principal direction is assumed to be:

$$u(x,,t) = U_{nm}\cos(n)e^{\text{jt} \blacklozenge \text{jk}_{nm}x + j\blacklozenge/2} \quad n=1\ m=1$$

$$v(x,,t) = V_{nm}\sin(n)e^{\text{jt} \blacklozenge \text{jk}_{nm}x} \quad n=0\ m=1$$

$$w(x,,t) = W_{nm}\cos(n)e^{\text{jt} \blacklozenge \text{jk}_{nm}x} \quad n=0\ m=1$$

where *n* and *m* correspond respectively to the azimuthal and axial modal order. Substituting in the equations of motion, assuming no force acting on the system, we obtain an eigenvalue problem whose solution is usually plotted in the so-called *dispersion curves* (wave number *kns as a function of frequency).*

In the case of finite length cylinders, the procedure previously described can be applied to derive modes shapes, natural frequencies and forced response of the system. In this case, we consider a cylinder of length *L* that is simply supported at the two ends (radial displacement, bending moment, torsional displacement and shear force in these points are zero). The radial displacement is:

$$w_{nm}(x,,t) = 2\,jW_{nm}\cos(n)\sin(k_{nm}x)e^{ijt}$$

and the corresponding eigenvalue is:

$$k_{nm} = m\blacklozenge / L$$

that again can be used to plot the dispersion curves for this configuration.

This analysis is fundamental for the design of the test rig in order to evaluate the frequency range of interest and the normal modes that can be excited using the piezoelectric actuators. Moreover, in order to measure any changes in the aerodynamic drag, it is necessary to constrain the cylinder in such a way that it is possible to measure the displacement in the axial direction. This can be realized by supporting the cylinder on tow points along its axis and inserting a load cell in between the constraint points and the supporting structure.

The cylinder chosen for this work has the following properties:

Low thickness to diameter ratio (0.009).

8" diameter to guarantee access to the inside and enough room for pressure probes, accelerometers, actuators and load cells.

Aluminum alloy.

These characteristics also assure that the circumferential modes that we are interested in are at low frequency as confirmed by the modal hammer analysis and the plot of the dispersion curves for the cylinder shown in Figure 1. The circumferential mode order is equivalent to circumferential wavenumber and is calculated by performing a spatial Fourier transform on the measurements around the cylinder. The red sections of the contour plot represent regions of high level and correspond to circumferential modes i.e. where an integer number of wavelengths fit into the circumference. These modes can then be targeted as potential drive frequencies for the traveling wave system.

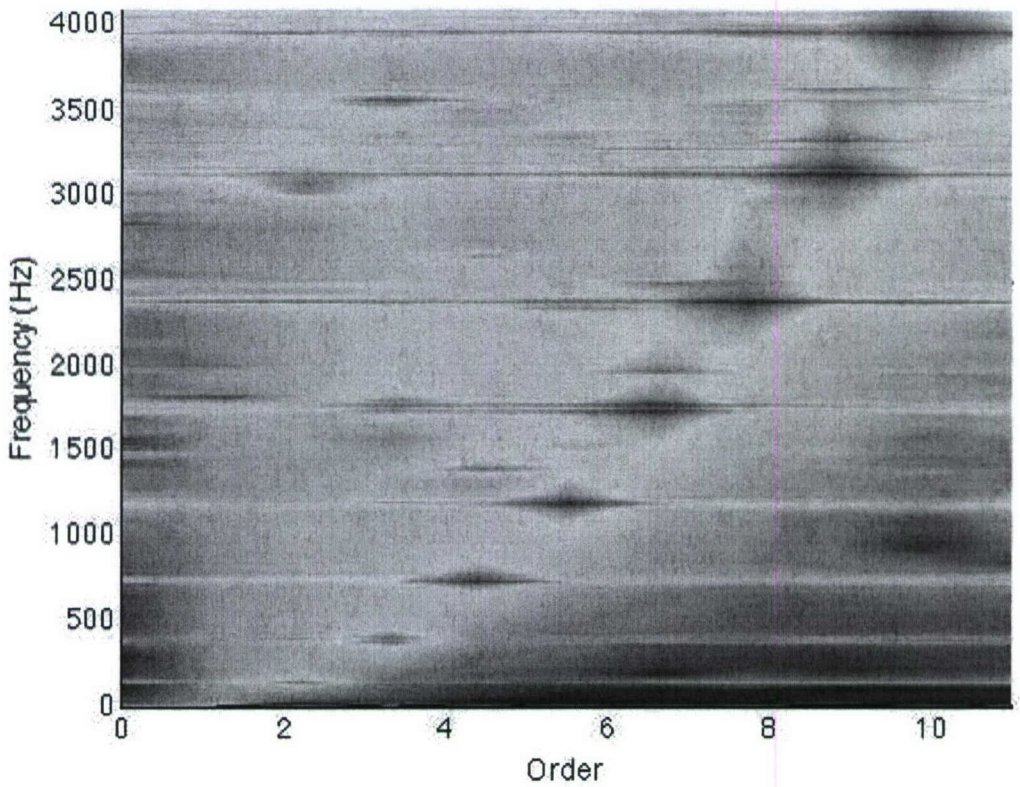


Figure 1: Measured mode order (or equivalently circumferential wavenumber) vs frequency for the cylinder used.

## TESTING AND CHARACTERIZATION OF STRUCTURAL WAVEGUIDE DESIGN

This document describes briefly the test rig used to demonstrate the possibility to drive circumferential traveling waves in a cylinder that interacts with the boundary layer in order to reduce turbulent drag. After a description of the test rig, the theory behind generating circumferential waves in cylindrical structures is presented and the system identification procedure is illustrated.

### TEST RIG DESCRIPTION

The test rig is an aluminum pipe described in Figure 4. The cylinder is cantilevered on a rigid support. It is equipped with 7 piezoceramic actuators equally spaced along a circle at a location

that is half of its length. The cylinder is internally supported by means of 4 load cells on a rigid beam as depicted in Figure 2. The load cells are placed in such a way to measure the axial load. In order to uncouple the shear drag on the cylinder from the pressure acting on the front surface, the front blunt body has been mounted directly on the supporting beam by means of a screw and the gap in between the cylinder and the blunt body has been filled with grease. A detailed drawing of the front part of the test rig is reported in Figure 3.

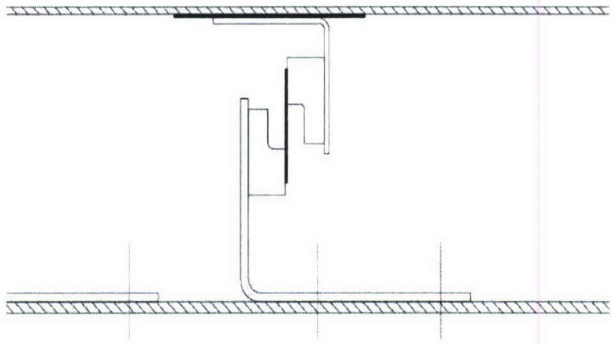

Figure 2. Detail of load cell

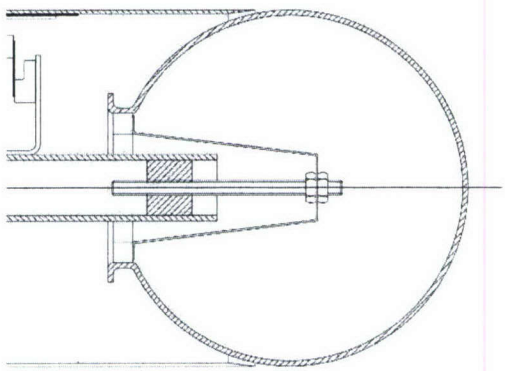

Figure 3. Detail of front blunt body

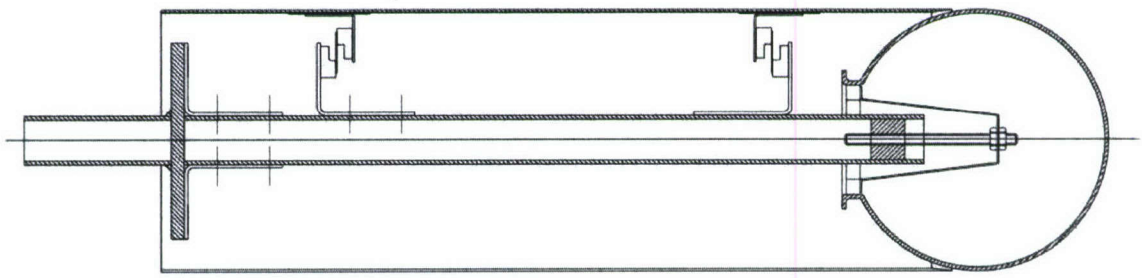

Figure 4. Test rig: lateral section

## CIRCUMFERENTIAL WAVES IN CYLINDERS

Every actuator *i* is driven with a sine wave and produces a pair of waves traveling in opposite

direction whose expression is:

$$w_i^{+}(,t)= e^{+ jm\varphi + jt \varphi jmi}$$

Equation 4

$$w^{\varphi}(,t)= e^{\varphi\ jm\varphi + jt + jmi\ i}$$

The quantity $w$ in Equation 5 is the radial displacement and is a complex number; in order to have the real displacement it's sufficient to take its real part. The term θ is the angular coordinate with respect to the positive x axis, ω is the angular frequency and $\varphi_i$ is the angular position of the $i$-th actuator. The parameter $m$ is the order of the circumferential mode. Then Equation 4 is valid only for normal modes since the wave spatial pattern has a wavelength that is a multiple of the perimeter. In this case ω is the natural angular frequency of the mode. When the system is excited with a harmonic function at ω the two waves generate a standing wave that is by definition a normal mode of the system. Each actuator is able to excite the same mode but since it has a $\varphi_i$ angle, normal modes have the same shape (if $m$ is fixed) but they are shifted by $-m\varphi_i$. In the most general case of $N$ actuators driven at the same frequency but with arbitrary phase delay $\psi_i$ the expressions for the two waves in Equation 4 are:

$$w_i^{+}(,t)= e^{+ jm\varphi + jt \varphi jmi \varphi j\varphi i}$$

Equation 5

$$w_i^{\varphi}(,t)= e^{\varphi\ jm\varphi + jt + jmi + j\varphi i}$$

And when are all driven at the same time, the resulting displacement takes the form:

$$w(,t)= w_i^{\cdot}(,t)+w_i^{\varphi}(,t)$$

$$w(\varphi, t)= \varphi\ e^{+ jm\varphi + jt \varphi jm\varphi j\varphi \cdot\ \varphi jm\varphi + jt + jm\varphi + j}$$

Equation 6

$$\begin{matrix} NN \\ ii \\ i=1\ i=1 \end{matrix}$$

Rearranging Equation 6, we have:

$$w(,t)= e^{jt} e^{+ jm} e^{\varphi\ jmi \varphi j\varphi i} + e^{\varphi\ jm} e^{jmi + j\varphi i}$$

$$\begin{matrix} \varphi\ NN \\ i\ i=1\ i=1 \end{matrix}$$

Equation 7

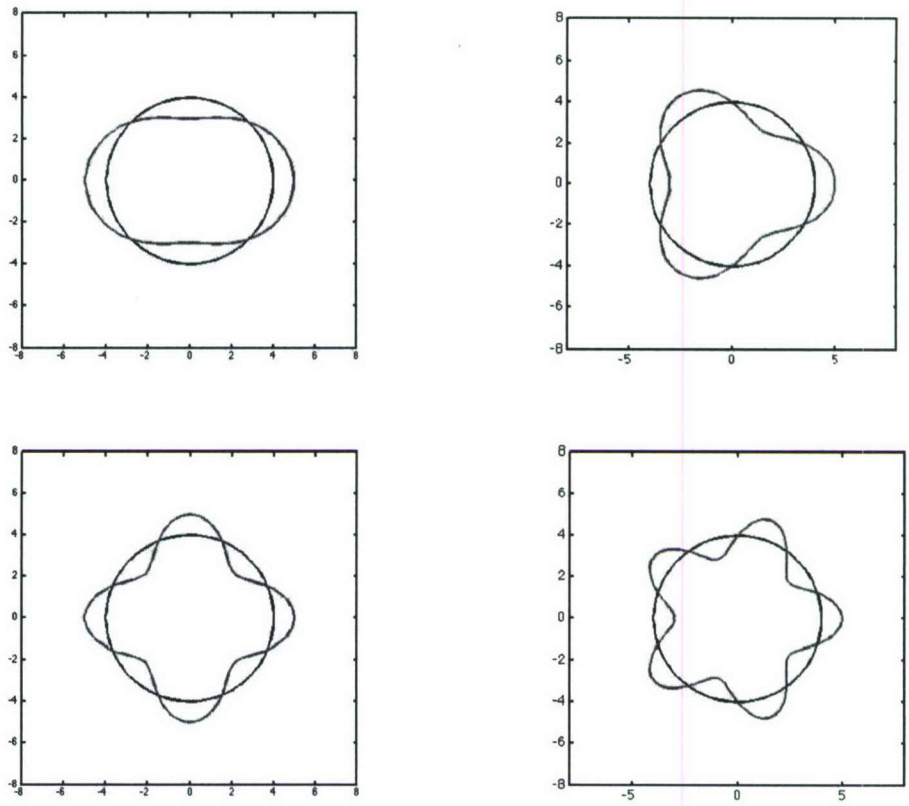

Figure 5. Examples of circumferential modes (k = 2,3,4,5)

## TRAVELING WAVES

In order to have a traveling wave, the radial displacement in every point on the circumference has to be:

$$w(,t) = \cos(m\theta + t)$$

this can be seen as the real part of a complex signal such as:

$$w(,t) = \mathrm{Re}(\cos(m\theta + t) + j\sin(m\theta + t))$$

that in the complex exponential notation is:

$$w(,t) = \mathrm{Re}(e^{j(t + jm\theta)})$$

This is equivalent to a positive traveling wave generated by an actuator placed at $\psi = 0$. Then, in order to generate a traveling wave, we have to suppress the one of the two waves (depending on the desired spinning direction). This can be done opportunely phasing the signal that drives each actuator; this means that the first sum in (4) should go to 1 while the second should go to zero. Since the two terms are equal, except for their signs, we choose to put to zero every exponent. In this way the two sum goes to *N* when we set:

$$w(,t) = \mathrm{Re}(N(\cos(m) + j\sin(m) + \cos(m) - j\sin(m))e)$$

Equation 8 $\quad - i = mi \quad i$

Then equation (3) becomes:

Equation 9 $\quad w(,t) = Ne^{\,t}(e^{jm} + e^{-jm})$

and the real displacement is:

$$w(,t) = 2N\cos(m)\cos(t)$$

Equation 10 $w(,t) = \mathrm{Re}(2N\cos(m)(\cos(t) + j\sin(t)))$

## TEST RIG CHARACTERIZATION

In order to establish the real properties of the cylinder, a system characterization has been performed when the system is in its final configuration (cantilevered on rigid support, with all the sensors and wires installed and the front and rear blunt bodies). The scope of the system identification is mainly to plot the dispersion curves and verify how the supports are influencing the ideal free-free boundary conditions. Two different tests have been carried out:

modal roving tap test (for dispersion curves)
system transfer function (point acceleration along cylinder axis and piezoelectric actuator excitation)

## MODAL ROVING TAP TEST

In this test the cylinder transfer functions have been measured in a point on the, tapping with a modal hammer in 21 equally spaced points along the circumference of the cylinder (this is the so-called roving technique and is well founded under the assumption that the principle of reciprocity is valid). The force and acceleration data is sampled at 8192 Hz and the transfer functions are averaged over 5 tests and collected (every transfer function is computed using a 8192 coefficients FFT in order to have a 1 Hz resolution on the frequency spectrum). The dispersion curves are derived computing the spatial FFT on the collected data.

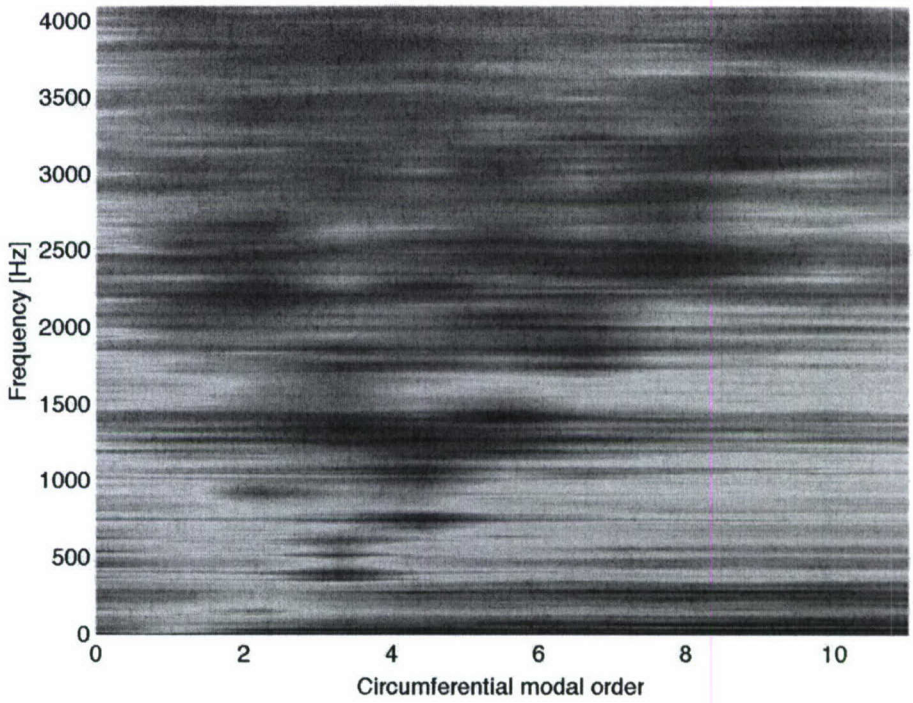


Figure 6. Dispersion curve

## SYSTEM TRANSFER FUNCTION ALONG AXIS

In order to verify the system response along the axis of the cylinder, the transfer function between the acceleration taken in 24 positions and the voltage driving one of the piezoceramic actuators have been taken. The results are presented in Figure 7. Transfer function along axis where location 1 is referred to the cylinder aft while 24 is the front.

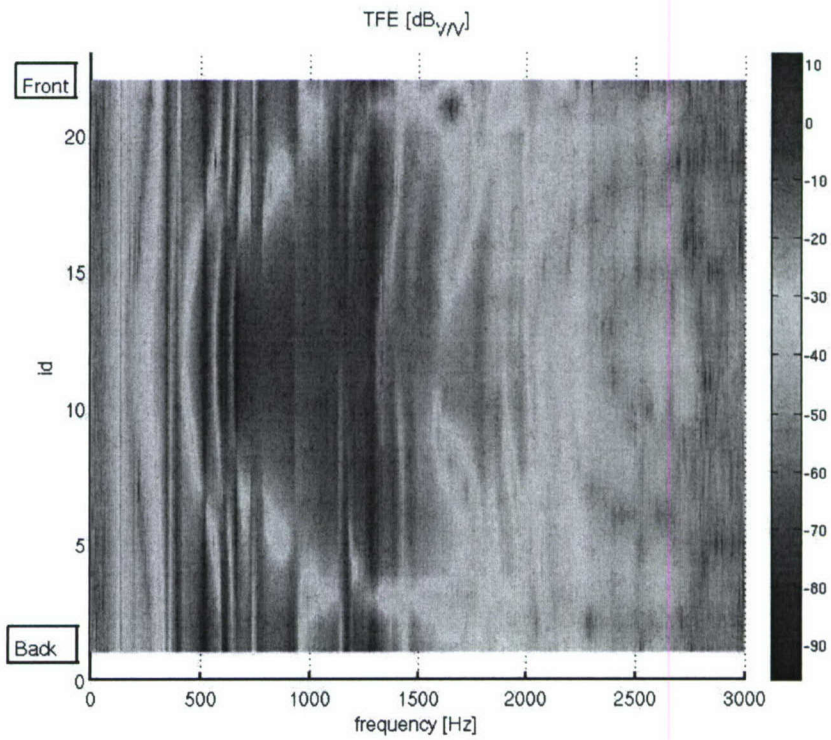

Figure 7. Transfer function along axis

It's clear that the first and the second circumferential modes, respectively at 129 and 355 Hz have the same axial wave number (equal to one) while other modes, for example at 500 Hz, have an higher $k_a$ that result in nodal lines at certain axis location. Observing the system response in those points will lead to a poor signal while position 12 is a good observation point for all modes.

## EXPERIMENTAL SETUP

Every actuator is driven by a PCB 790 series amplifier. Every channel can drive a capacitive load such as a piezoceramic actuator, at 200 V peak to peak and 200 mA. The frequency bandwidth depends on the load itself and with the installed actuators it's up to 1.2 kHz. The control software has been developed in C on a Linux/RTAI platform. A GTK+ user interface controls the real time code and sets up the communication with two data acquisition boards (namely a National Instrument NI 6143 for analog to digital conversion and a NI 6733 for analog outputs). The code allows setting the sampling frequency, the number of channels to drive and the parameters of the driving signal (amplitude, frequency and phase). The phase is automatically calculated while the frequency is derived from a configuration file that has been compiled according to the system identification procedure (and in particular from the dispersion curves in Figure 6 whose summary is here reported in table 1.

Table 1. Modes frequency and order

| Mode order | Frequency Hz |
|---|---|
| 2 | 129 |
| 3 | 355 |
| 4 | 745 |

## PRELIMINARY FLOW VISUALIZATION AND PARTICLE IMAGE VELOCIMETRY RESULTS

### PARTICLE IMAGE VELOCIMETRY BACKGROUND

The range of applications and current advancements of DPIV is so vast and diverse that a detailed review is impossible in itself. We will however address the DPIV contributions that pertain to the development of our in-house developed TRDPIV methodology that was used during this effort. Review articles by Adrian[37] and Grant[38] provide comprehensive summaries of the principles of the method and its various applications. The work of Willert and Gharib[39], Westerweel[40,41], and Huang et al.[42] established the digital implementation of PIV. Further developments resulted in super-resolution, iterative, and hybrid DPIV algorithms that increased accuracy and spatial resolution[43-46]. For iterative DPIV methods the use of a discrete-window offset (DWO) was introduced[47]. The combination of iterative DPIV with DWO significantly reduces the spatial averaging effects, improves resolution and accuracy, and renders the uncertainty independent of the total measured displacement. The accuracy is further improved by the use of an adaptive Central Difference (CDI) second order DWO[48]. This is especially important for vortical flows and systems with large pulse separation such as μDPIV and TRDPIV systems.

Despite the advances in improving the spatial resolution and accuracy of the method, conventional DPIV systems provide a limited temporal resolution (<30Hz), which is insufficient for resolving turbulent flow fluctuations. Previous implementation of time-resolved systems employed digital cameras with limited resolution[49] or drum film cameras that are limited in recording times[50]. Vlachos[51, 52] presented one of the very first fully digital systems that extended the sampling frequency to 1 kHz with 256x256 pixel spatial resolution. Recently Upatnieks et al.[53] presented a kHz frame-rate analog PIV system capable of 4000 frames/s (fps) for 0.5s maximum recording. Analog recording delivers superior spatial resolution (>1Kx1K). However, due to the high frame rates the extreme rotation speed for the film compromises the image registration. This significant error source is superimposed on the common digitization errors.
Vlachos and collaborators recently developed a TRDPIV system with 1-10 kHz sampling rate and extended recording time, capable of resolving the spatio-temporal evolution of turbulent flow, improving upon the earlier works of Scarano & Riethmuller[54], Wereley & Meinhart[48], Guezennec & Kiritsis[44], and Cowen & Monismith[46]. Improvements on the method increased the accuracy for resolving vortical, near-wall and poly-dispersed multi-phase flows[55]. We introduced a novel hierarchical scheme that is computationally efficient and has showed great potential for high shear vortical flows by alleviating the large spatial averaging effects of multigrid approaches. A new hybrid particle tracking method based on an adaptive cross-correlation masking was also introduced. Detailed error analysis by our group characterized the performance of the system and compared its accuracy with commercial and other established algorithms[56]. Error analysis results, using Monte-Carlo simulations of an ideal vortex, comparing our method with conventional multigrid DPIV showed that the overall accuracy especially under high shear rates was improved by 60%. These results clearly illustrated the advantages of our methodology, particularly for resolving vortical flows.

Although during the past few years commercial TRDPIV systems have become available, successful implementations of the method are limited. One reason is the prohibitive cost of these TRDPIV systems. More importantly, TRDPIV measurements are not trivial. Severe limitations, including the very low pulse energy of the available high frequency lasers and accurate timing of the time separation between image pairs, restrict the applicability of the method to a few types of -mainly low speed-flows and require meticulous experimentation. It is beyond the scope of this text to provide a detailed technical description of these issues. The PI was one of the first to deliver kHz TRDPIV measurements over a variety of applications[51,52,5556-59] and has published over 90 refereed conference and journal papers related method development and implementation.

After two equipment upgrades we are currently operating a stereoscopic TRDPIV system with 0-10kHz sampling rate and 1μs minimum inter-frame time delay. In addition, 3 IDT X-Stream CMOS cameras with 1280x1024 pixel resolution at 1 kHz sampling rate are used for the image recording. CMOS cameras are preferred for TRDPIV systems as they deliver better performance at high frame rates at a much lower cost compared to CCD's. Moreover, signal to noise ratio of current CMOS sensors is very comparable to CCDs. The Stereo DPIV implementation used in our system is based on the work by Prasad & Adrian[60]. In conclusion, the DPIV system employed herein is one of very few available worldwide to deliver kHz rate Time-Resolved Stereo DPIV, it involves the latest available instrumentation and it extensively tested and benchmarked over a wide variety of flows.

## PRELIMINARY TRDPIV EXPERIMENTAL VALIDATION

Due to time constrains and limitation of resources, at the time of this report the TRDPIV study was not completed therefore all results shown here are merely representative of the

measurement capabilities. Ongoing experimental results and further analysis of these efforts will be disseminated at a later time in the form of conference proceedings and archival publications.

## EXPERIMENTAL METHOD

A TRDPIV experimental study was performed in order to quantitatively visualize the effect on the flow of driving circumferential travelling waves around the wall of a cylinder. The effect of travelling waves under quiescent flow conditions was investigated. The experimental methods and procedures are explained and some preliminary findings are demonstrated.

An in-house customized TRDPIV system was employed in order to quantitatively visualize the flow very close to the wall of the travelling wave cylinder. A series of instantaneous velocity fields were generated using this technique. Figure 8 (left) provides a view of the experimental setup. It includes a New Wave Nd-YAG laser, which produces approximately 1.5 centimeter wide and 2 millimeter deep laser sheet with the use of properly placed optics. The cylinder is located inside a plenum in order to keep the particle seeding dense enough for PIV. Flow was seeded with pulverized 90% solution of Di-2-Ethylhexel Sebecat using the Lavision seeder shown in Figure 8 (right).

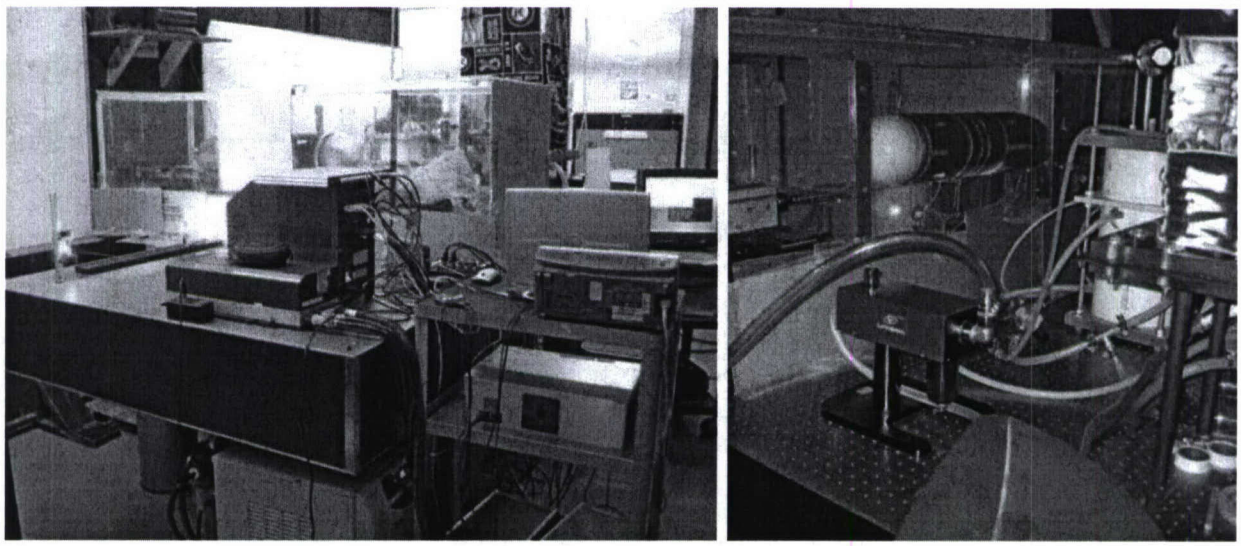

Figure 8. (a) View of the TRDPIV experimental setup (b) cylinder structure and seeder

Implementing the method described earlier, a structural travelling wave is applied around the circumference of an aluminum cylinder in a clockwise direction by the use of 7 equally spaced piezoceramic actuators. The cylinder was forced with a travelling wave at its third circumferential mode which is demonstrated in Figure 9.

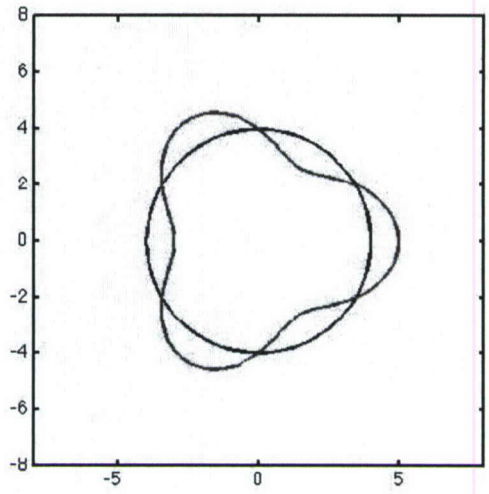


Figure 9. The third circumferential mode shown above was used

An IDT MotionPro X5 digital CCD camera was used to acquire images. A special optical component called a GRINscope was used with the camera. This is an in house developed and customized borescopic imaging system based on a cylindrical lens with radially varying index of refraction. This enables it to transmit the light with high efficiency and minimal distortion. This component made it possible to achieve a magnification of approximately 30 μm per pixel without needing to place the camera close to the laser sheet. A closer view of the GRINscope and the region of interest is shown in Figure 10. The resulting magnification was sufficient to resolve the micron size structural deflections on the surface of the cylinder.

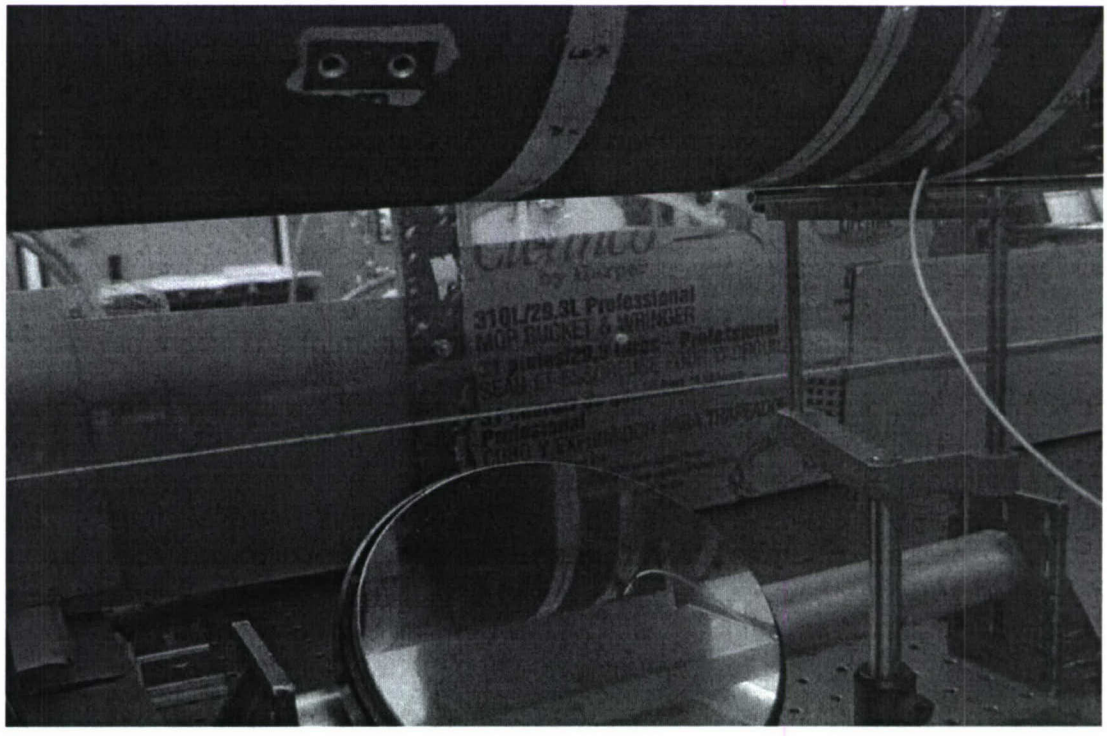

## RESULTS

Figure 11 through Figure 13 show the velocity fields at three successive time instants. At the first instant, shown in Figure 11, the cylinder wall is forced by the travelling wave to move to the location designated by the dashed curve. As expected there is a strong flow away from the wall. In the next time instant shown in Figure 12, the cylinder wall retreats to its original location designated by the solid curve, and there is a flow in the clockwise direction around the circumference of the cylinder wall. At the time instant shown in Figure 13, the flow decelerates and reaches also quiescent conditions.

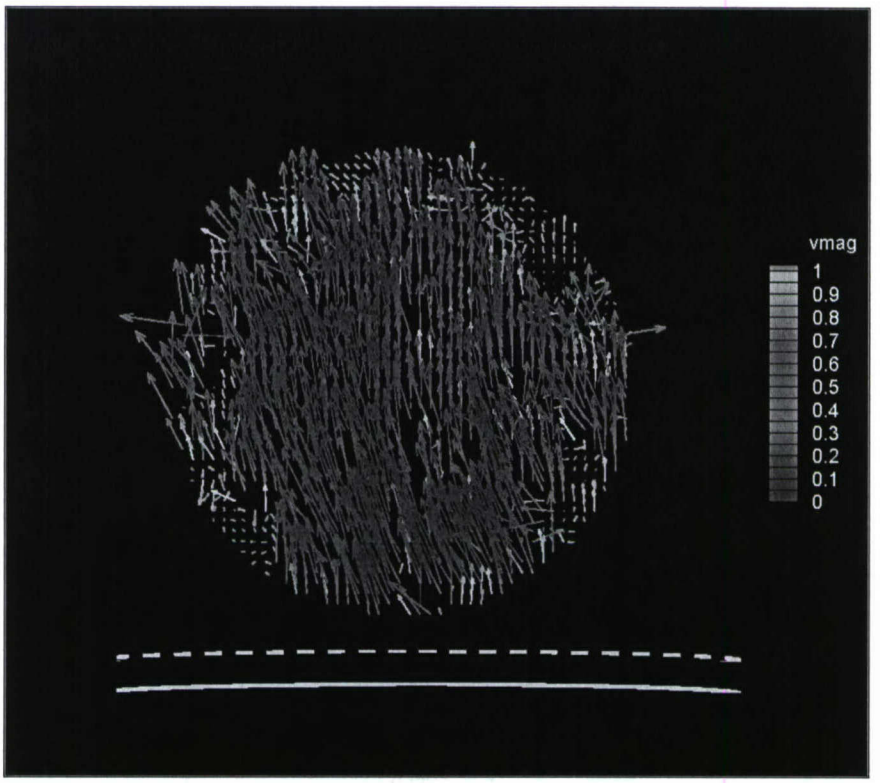


Figure 11. First time instant, fluid is being pushed away the wall by the wall's movement.

Images were acquired at 200Hz sampling rate. Acquired images were processed by using the FlowIQ software developed by Aeroprobe cooperation. FFT based correlation technique was employed using 16 x 16 pixel interrogation windows. Iterative and discrete window offset (DWO) method were used along with adaptive central difference DWO algorithms in order achieve higher accuracy for a near-wall flow condition.

RESULTS

Figure 11 through Figure 13 show the velocity fields at three successive time instants. At the first instant, shown in Figure 11, the cylinder wall is forced by the travelling wave to move to the location designated by the dashed curve. As expected there is a strong flow away from the wall. In the next time instant shown in Figure 12, the cylinder wall retreats to its original location designated by the solid curve, and there is a flow in the clockwise direction around the circumference of the cylinder wall. At the time instant shown in Figure 13, the flow decelerates and reaches also quiescent conditions.

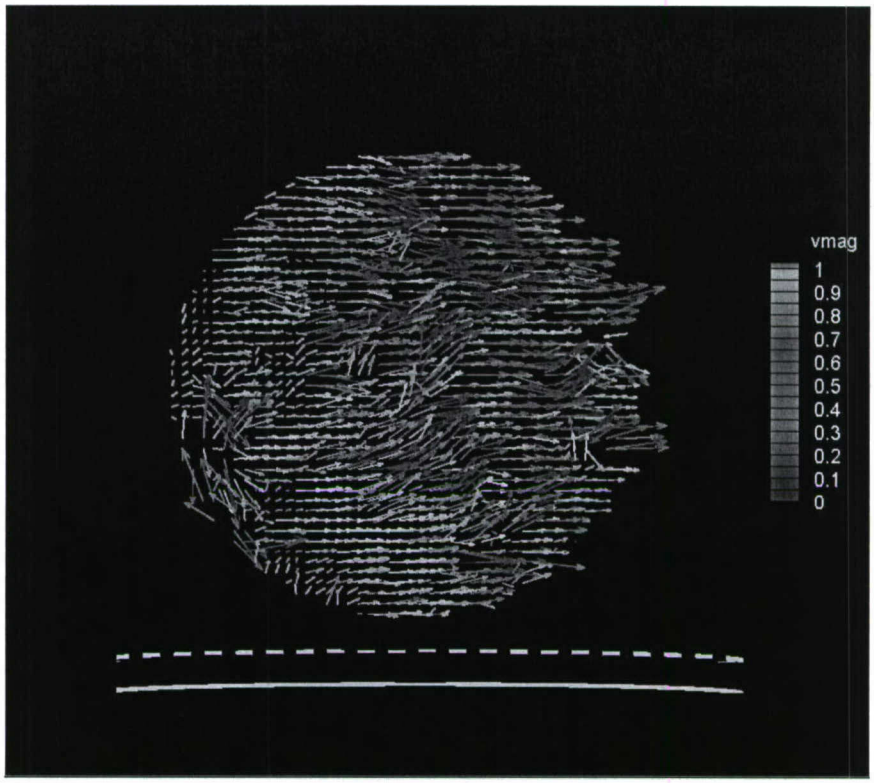


Figure 12. Second time instant, there is a flow in the clockwi

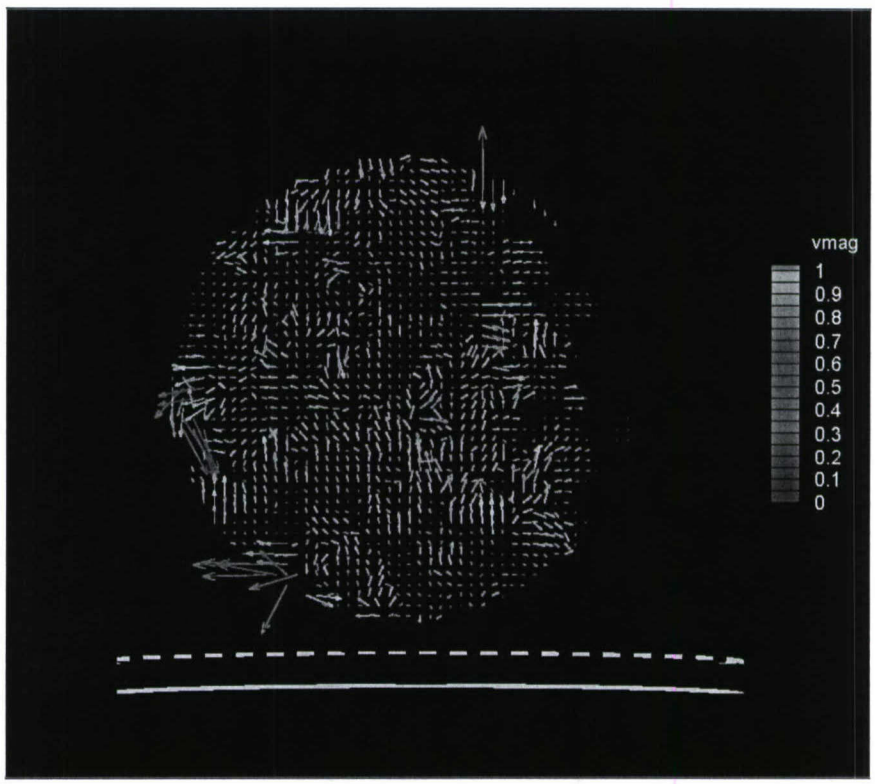


Figure 13. Third time instant, flow is steady.

Figure 12. Second time instant,there is a flow in the clockwise direction.

## CONCLUSIONS AND FUTURE WORK

During the nine month performance of the work presented herein we were successful in designing developing and fabricating structural waveguides within a cylindrical structure. Structural characterization of the prototype demonstrates that the performance was within the design expectation. Subsequently aerodynamic testing was initiated in order to validate that the proposed concept can impart flow disturbances that reduce turbulent viscous drag. At the time of this report only quantitative flow visualization under quiescent flow conditions had been performed and preliminary analysis of the results is presented. The PIV results showed a three stage cycle occurring, which creates a motion that sweeps the flow very close to the wall in a clockwise direction. This movement of fluid might interrupt the near-wall turbulence production

and reduce the viscous drag. Future work on this project should include drag measurements in an air tunnel in order to see the effect of travelling wave on the drag measurements.

## REFERENCES


Townsend, A. "The Structure Of Turbulent Shear Flow," Cambridge University Press, 1976.

[2] Head, M. and Bandyopadhyay, P. Journal Of Fluid Mechanics, 107, 297, 1981.

[3] Perry, A. and Chong, M., Journal Of Fluid Mechanics, 119, 173, 1982.

[4] Karniadakis and Choi (2003): Mechanisms of transverse motion in turbulent boundary layers, Ann. Rev of Fluid Mechanics Vol. 35: 45-62.

[5] Bechert, D. and Bartenwerfer, M., Journal Of Fluid Mechanics, 206, 105, 1992.

[6] Walsh MJ. 1980. Drag characteristics of Vgroove and transverse curvature riblets. In Viscous Drag Reduction, ed. GR Hough, pp. 168–84. Washington, DC: AIAA.

[7] Walsh MJ. 1982. Turbulent boundary layer drag reduction using riblets. AIAA Pap. 82-0169.

[8] Walsh MJ. 1990. Riblets. In Viscous Drag Reduction in Boundary Layers, Progress in Astronautics and Aeronautics, ed. D Bushnell, J Hefner, pp. 123. Reston, VA: AIAA.

[9] Jung WJ, Mangiavacchi N, Akhavan R. 1992. Suppression of turbulence in wall-bounded flows by high frequency spanwise oscillations. Phys. Fluids A 4:1605–7.

[10] Choi KS, DeBisschop JR, Clayton BR. 1998. Turbulent boundary layer control by means of spanwise-wall oscillation. AIAA J. 36:1157–63.

[11] Choi KS, Graham M. 1998. Drag reduction of turbulent pipe flows by circular-wall oscillation. Phys. Fluids 10:7–9.

[12] Choi KS, Clayton BR. 2001. The mechanism of turbulent drag reduction with wall oscillation. Int. J. Heat Fluid Flow 22:1–9.

[13] Jimenez J, Pinelli A. 1999. The autonomous cycle of near-wall turbulence. J. Fluid Mech. 389:335–59.

[14] Schoppa W, Hussain F. 1997. Genesis and dynamics of coherent structures in near-wall

turbulence. Proc. Self-Sustain. Mech. Wall Turbul., ed. R Panton, pp. 385–422. Comput.Mech. Publ.

[15] Schoppa W, Hussain F. 1998.Alarge-scale control strategy for drag reduction in turbulent boundary layers. Phys. Fluids A 10:1049–51.

[16] Schoppa W, Hussain F. 2002. Coherent structure generation in near-wall turbulence. J. Fluid Mech. 453:57–108.

[17] Du, Y., V. Symeonidis, G. Karniadakis (2002) "Drag reduction in wall-bounded turbulence via a transverse travelling wave" Journal of Fluid Mechanics, 457: 1-34

[18] Du, Y and Karniadakis, G., (1999) Science, vol. 288.

[19] Park. J., Henoch, C., McCamley, M., & Breuer, K. S. "Lorentz Force Control of Turbulent Channel Flow". AIAA Paper 2003-4157. Orlando, FL. June, 2003.

[20] Breuer, K.S., Park, J. & Henoch, C. "Actuation and Control of Turbulent Channel Flows using Lorentz Forces" Physics of Fluids (in review) 2003.

[21] Rediniotis O. K., D.C. Lagoudas , R. Mani and G.E. Karniadakis, "Active Skin for Turbulent Drag Reduction", SPIE's 9th Annual International Symposium on Smart Structures and Materials, (San Diego, CA), 2002.

[22] Leissa, A.,"Vibration of Shells,"ASA/AIP Press, 1993.

[23] Fahy, F.,"Sound and Structural Vibration," Academic Press, London, 1985.

[24] Victor Giurgiutiu,"Review of Smart-Materials Actuation Solutions for Aeroelastic and Vibration Control,"Journal of Intelligent Material Systems and Structures, Jul 2000; 11: 525 -544.

[25] Mary I. Frecker,"Recent Advances in Optimization of Smart Structures and Actuators,"Journal of Intelligent Material Systems and Structures, Apr 2003; 14: 207 216.

[26] Carneal, J. P. and Fuller, C. R., "An Analytical and Experimental Investigation of Active Structural Acoustic Control of Noise Transmission through Double Panel Systems" Journal of Sound and Vibration, Volume 272, Issues 3-5, 6 May 2004, Pages 749-771.

[27] Lalande, F., Chaudhry, Z., Rogers, C. A., 1995, "Comparison of Different Impedance-Based Models for Out-of-Phase Actuation of Actuators Bonded on Ring Structures," Journal of

Intelligent Material Systems and Structures, Vol. 6, May, pp. 389
395.

28

Lalande, F., Chaudhry, Z., Rogers, C. A., 1995b, "Impedance Based Modeling of actuators Bonded to Shell Structures," Journal of Intelligent Material Systems and Structures, Vol. 6, November, pp. 389-395.

29

Carneal, J. P. and Fuller, C. R., "A Biologically Inspired Controller," Journal of the Acoustical Society of America, Vol. 98(1), July 1995, pp. 386-396.

30

Carneal, J. P. and Fuller, C. R., "A Biologically Inspired Controller for Sound Applications," AIAA Journal, Vol. 33, No. 5, May 1995, pp. 794-797.

31

A. Purekar, D. Pines, "A Phased Sensor/Actuator Array for Detecting Damage in 2-D Structures," AIAA Paper No. AIAA-2002-1547

32

Marty E. Johnson and Chris R. Fuller, "Creating high level sound in a duct using an axial array of sources," Journal of Sound and Vibration, Vol. 277(1-2), pp101-122, (Oct 2004)

33

D. Duhamel, B.R. Mace and M.J. Brennan,"Finite element analysis of the vibrations of waveguides and periodic structures"Journal of Sound and Vibration, Volume 294, Issues 1-2, 27 June 2006, Pages 205-220.

34 Ivan Bartoli, Alessandro Marzani, Francesco Lanza di Scalea and Erasmo Viola,"Modeling wave propagation in damped waveguides of arbitrary cross-section Journal of Sound and Vibration, In Press, Corrected Proof, Available online 20 March 2006.

35

R. Langley,"Wave Evolution, Reflection, and Transmission along Inhomogeneous Waveguides," Journal of Sound and Vibration, Volume 227, Issue 1, 14 October 1999, Pages 131-158.

36

Marty Johnson, Brad Batton,"Wave Based Optimization of Distributed Vibration Absorbers," NOISE-CON 2005, Minneapolis, Minnesota, 2005 October 17-19.

37 Adrian, R. J. (1991): Particle-imaging techniques for experimental fluid mechanics. ARFM, 23, 261-304.

38

Grant, I. (1997): Particle image velocimetry: A review. Proc., Institute of Mechanical Engineers.

39 Willert, C. E. and Gharib, M. (1991): Digital particle image velocimetry. Experiments in Fluids, 10, 181-193.

40

Westerweel, J. (1993a): Digital Particle Image Velocimetry, Theory and Application. Delft University Press, Delft, The Netherlands.

41

Westerweel, J. (1993b): Analysis of PIV interrogation with low pixel resolution. In Optical diagnostics in fluid and thermal flow, (ed) Trolinger J. D., Proc SPIE Vol. 2005, pp. 624635.(San Diego July 1993).

42

Huang, H. T. D. Dabiri and Gharib, M. (1997): On Errors of digital particle image velocimetry. Meas. Science and Technology, .8, 1427-1440.

43

Scarano, F. and Rieuthmuller, M. L. (1999): Iterative multigrid approach in PIV image processing with discrete window offset. Experiments in Fluids, 26, 513-523.

44

Guezennec YG and Kiritsis N (1990): Statistical investigation of errors in particle image velocimetry. Experiments in Fluids, 10, 138-146.

45

Keane RD, Adrian RJ, Zhang Y (1995): Super resolution particle image velocimetry., Meas. Science and Technology, .6, 754-768.

46

Cowen B and Monismith S (1997): A hybrid digital particle tracking velocimetry technique. Experiments in Fluids, 22, 199-211.

47

Westerweel, J. (1997): The effect of a discrete window offset on the accuracy of cross-correlation analysis of digital PIV recordings. Experiments in Fluids, 23, 20-28.

48

Wereley ST, Meinhart CD (2001): Second-order accurate particle image velocimetry. Experiments in Fluids, 31, 258-268.

49

Whybrew A, Reeves M, Slagle RL, Boaler JJ, Baughan AK, Nicholls TR, Towers DP, Tavender B, Buckberry CH (1999): Two techniques for all-digital time-resolved PIV. Third International Workshop on Particle Image Velocimetry. (Santa Barbara, 16-18 Sept 1999).

50

Lecordier B and Trinite M (1999): Time resolved PIV measurements for high speed flows. Third International Workshop on Particle Image Velocimetry. (Santa Barbara, USA).

51

Vlachos P. P., Donnelly M. J. and Telionis D. P., "On the Wake of a Circular Cylinder Piercing a Water Free Surface", *ASME Fluids Engineering Division Summer Meeting*, FEDS98-5177, 1998.

52

Vlachos, P., "An Experimental Spatio-Temporal Analysis Of Separated Flows Over Bluff Bodies Using Quantitative Flow Visualization," PhD. Dept. of Eng. Science and Mechanics, Virginia Tech, Blacksburg, VA, 2000.

53

Upatnieks A., Laberteaux K., Ceccio S. L. (2002):A kilohertz frame rate cinematographic PIV system for laboratory-scale turbulent and unsteady flows. Experiments in Fluids, 32, 87-98.

54

Scarano, F. and Rieuthmuller, M. L. (1999): Iterative multigrid approach in PIV image processing with discrete window offset. Experiments in Fluids, 26, 513-523.

55

Abiven, C, Vlachos PP. Super spatio-temporal resolution, digital PIV system for multi-phase flows with

phase differentiation and simultaneous shape and size quantification, Int Mech Eng Congress, Nov. 17-22, New Orleans, LA, 2002.

[56] Abiven C, Vlachos PP and Papadopoulos G. DPIV Strategies for resolving high shear and vortical flows. Int Mech Eng Congress, Nov. 17-22, New Orleans, LA, 2002.

[57] Vlachos P. P. and Hajj M. R., "A Time-Resolved DPIV Study Of The Unsteady Character Of The Flow Over A Surface Mounted Prism" Journal Of Wind Engineering and Industrial Applications. vol 90 pp 543-553, 2000

[58] P. P. Vlachos, and D. P. Telionis, "Turbulence Characteristics In The Wake Of A Circular Cylinder Near The Free Surface", FEDSM2000-11320, Boston, MA, 2000

[59] P. P. Vlachos, and D. P. Telionis, "Three-Dimensional Streamwise Vortical Structures Of A Turbulent Wake Near The Free Surface." FEDSM2000-11262, Boston, MA, 2000.

[60] Prasad A.K. and Adrian R J (1993): Stereoscopic particle image velocimetry applied to liquid flows. Experiments in Fluids 15, 49-60.